ARTICLE

Self-Healing and Elastic Triboelectric Nanogenerators for Muscle Motion Monitoring and Photothermal Treatment

Dan Yang, Yufeng Ni, Xinxin Kong, Shuyao Li, Xiangyu Chen, Liqun Zhang, and Zhong Lin Wang*

Cite This: https://doi.org/10.1021/acsnano.1c04384

Read Online

ACCESS | Metrics & More | Article Recommendations | Supporting Information

ABSTRACT: Owing to wearing and unpredictable damage, the working lifetime of triboelectric nanogenerators (TENGs) is largely limited. In this work, we prepared a single-electrode multifunctional TENG (MF-TENG) that exhibits fast self-healing, human health monitoring capability, and photothermal properties. The device consists of a thin self-healing poly(vinyl alcohol)-based hydrogel sandwiched between two self-healing silicone elastomer films. The MF-TENG exhibits a short-circuit current, short-circuit transfer charge, and open-circuit voltage of 7.98 μA, 78.34 nC, and 38.57 V, respectively. Furthermore, owing to the repairable networks of the dynamic imine bonds in the charged layer and the borate ester bonds in the electrodes, the prepared device could recover its original state after mechanical damage within 10 min at room temperature. The MF-TENG can be attached to different human joints for self-powered monitoring of personal health information. Additionally, the MF-TENG under near-infrared laser irradiation can provide a photothermal therapy for assisting the recovery of human joints motion. It is envisaged that the proposed MF-TENG can be applied to the fields of wearable electronics and health-monitoring devices.

KEYWORDS: triboelectric nanogenerator, poly(vinyl alcohol), self-healing, health-monitoring, photothermal therapy
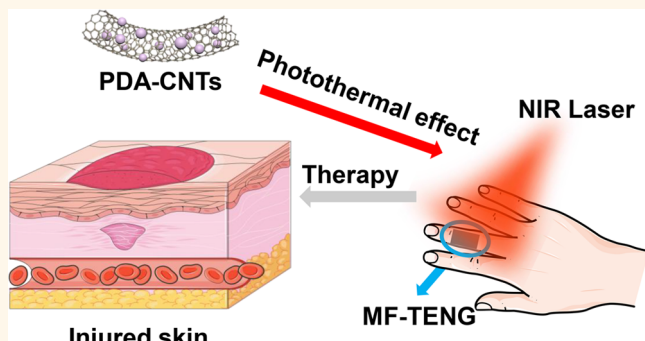
With the extensive development of modern microelectronic technology, stretchable, flexible, and human-friendly electronic devices have attracted increasing attention in recent years. Triboelectric nanogenerators (TENGs) based on the coupling between triboelectrification and electrostatic induction are an energy technology that can convert mechanical energy in the surrounding environment into electrical energy.[1−10] Owing to their high energy conversion efficiency, low cost, and the possibility of using diverse materials, TENGs have been widely utilized in various fields, such as wearable electronic devices,[11−13] Internet of things,[14,15] environmental sensors,[16,17] miniaturized sensors,[18−22] and medical treatment.[23−27] In addition, various types of TENG with excellent flexibility based on soft materials have been developed, such as assembled TENGs,[28] fabric-based TENGs,[29] paper-based TENGs,[30] and skin-based TENGs.[31] Therefore, the next generation of electronic devices will exhibit elastic properties[32−35] and will be biocompatible.[36,37] Motivated by the high demand for wearable devices, research groups have made extensive efforts to develop soft and wearable electronic devices. Different types of TENG that can monitor human health information have been reported based on the harvesting of mechanical motion energies from the human body. Park et al.[38] successfully fabricated an electrospun nanofiber based on polyvinylidene fluoride/MXene nanocomposites, which was used as a promising negative triboelectric layer for boosting the performance of harvesting triboelectric energy. This self-powered TENG sensor for foot motion could automatically control the step lights based on the human foot motion on stairs. Peng et al.[39] reported a breathable, biodegradable, and antibacterial e-skin based on an all-nanofiber TENG sandwiching a silver nanowire (NW) between polylactic coglycolic acid and poly(vinyl alcohol) (PVA). This e-skin could achieve self-powered monitoring of the physiological signal from the whole body as well as joint motion. However, scratching and interface friction can cause damage and performance loss in TENG
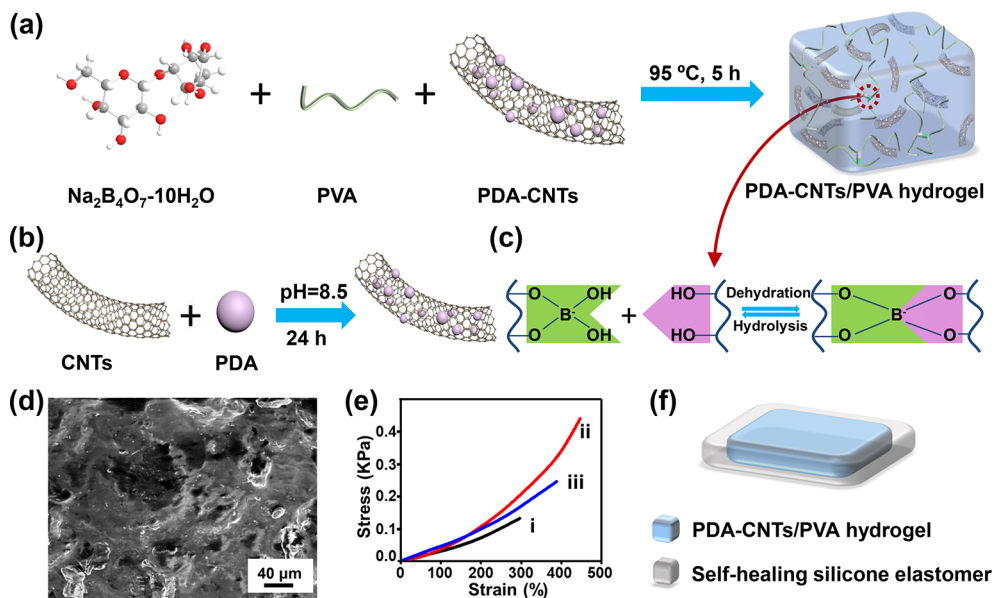
Figure 1. Illustration and characterization of the MF-TENG. (a) Preparation process of the PDA-CNTs/PVA hydrogel; (b) Schematic diagram of the PDA modification of CNTs; (c) Self-healing mechanism of the PDA-CNTs/PVA hydrogel; (d) SEM image of the PDA-CNTs/PVA hydrogel; (e) Stress−strain curves of (i) pure PVA, (ii) the original PDA-CNTs/PVA hydrogel, and (iii) the self-healed PDA-CNTs/PVA hydrogel; (f) Schematic structure of the MF-TENG.

devices, which would largely limit their long-term applications.[40,41] Preparing a self-healing TENG with high elasticity is considered to be a good strategy to solve the above problems. Xu et al.[42] reported a fully healable TENG which consisted of healable polydimethylsiloxane−polyurethane materials and healable magnetic-assisted electrodes. However, the self-healing process of this TENG required heating and magnetic electrodes, which resulted in the device being nonstretchable and inflexible. Sun et al.[43] reported a self-healing TENG that was obtained by sandwiching a silver NW/poly(3,4-ethylenedioxythiophene) composite electrode into a self-healing polydimethylsiloxane (PDMS) elastomer using dynamic imine bonds to repair the mechanical damages. Wang et al.[44] reported a versatile moist-electric film generator (MEFG) exhibiting transparency, self-healing, and flexibility. This MEFG consisted of a conductive Ag NW network as the electrode and a water-absorbing poly(4-styrene sulfonic acid) and poly(vinyl alcohol) composite (PSS−PVA) film as the electricity-generating active material. With the reconstruction of the damaged PSS−PVA film, which was driven by hydrogen bond interaction and the reconnection of the Ag NW layer via the van der Waals force, this MEFG could recover its original performance.

In this work, a single-electrode multifunctional TENG (MF-TENG) is proposed, whereby a thin PVA-based hydrogel, which consists of sodium borate and carbon nanotubes (CNTs) modified by poly(dopamine) (PDA), here referred to as PDA-CNTs, was sandwiched between two self-healing silicone elastomer films. The PVA hydrogel was chosen as the matrix owing to its environmental friendliness and good biocompatibility with the human skin. Sodium borate was dispersed into the PVA hydrogel matrix to provide reversible healing sites. At room temperature, the formation of dynamic borate bonds endows the hydrogel with self-healing capability. The PDA-CNTs were incorporated into the PVA hydrogel matrix to endow the film with high conductivity. PDA improves the dispersion of the PDA-CNTs in the PVA hydrogel matrix. In addition, the large amount of catechol and amino groups in PDA

can form reversible hydrogen bonds with the hydroxyl groups in PVA, which is beneficial for improving the self-healing ability of the PDA-CNTs/PVA hydrogel. The results show that the prepared MF-TENG could complete the self-healing process at room temperature within 10 min, which was accompanied by a completely recovered electrical output performance. Being a soft device, the MF-TENG was attached to different human joints to harvest energy from human motion and output electrical signals that can provide information about personal health. Furthermore, the PDA-CNTs in the PVA hydrogel provide the MF-TENG with an effective photothermal therapy, which would assist the recovery of human joints motion under near-infrared (NIR) laser irradiation. In addition, the MF-TENG displayed good shape-tailorable features, which could extend its application range as a wearable device.

RESULTS AND DISCUSSION

The preparation process and characterization of the MF-TENG are shown in Figure 1. PVA was used as the hydrogel matrix with the addition of sodium borate and the conductive PDA-CNTs to prepare the self-healing PDA-CNTs/PVA hydrogel. The detailed preparation process of the PDA-CNTs/PVA hydrogel is displayed in Figure 1a. The CNTs could determine the relative resistance change and provide the photothermal effect of the MF-TENG. Due to the large difference in surface energy between PVA and the CNTs, the CNTs usually gather together spontaneously to form aggregations in the PVA matrix, which would damage the flexibility of the MF-TENG. Therefore, dopamine (DA), which is the main ingredient of mussel adhesive proteins, was used to modify the surface of the CNTs to improve the interfacial compatibility between PVA and the CNTs. As shown in Figure 1b, in a weakly alkaline environment, the DA could spontaneously oxidize and polymerize to form a PDA network on the surface of the CNTs.[35] The thermogravimetric analysis (TGA) curves of the pristine CNTs and PDA-CNTs are shown in Supporting Information (SI) Figure S1. After heating to 800 °C, the mass residue of the pristine CNTs
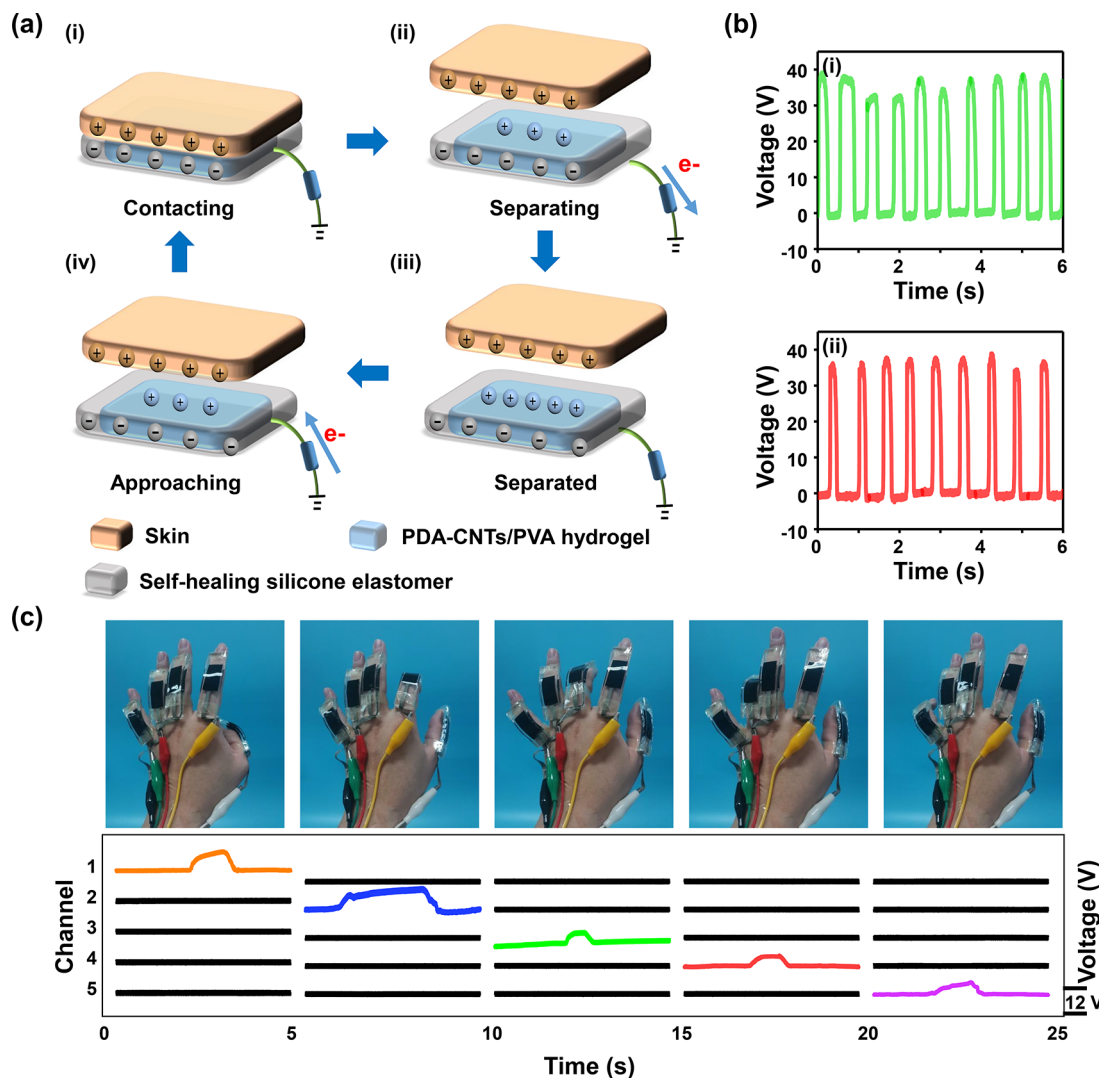
Figure 2. (a) Schematic illustration of the working mechanism of the MF-TENG in single-electrode mode; (b) Open-circuit voltage of (i) the original and (ii) the self-healed MF-TENG; (c) Real-time responses of the bending of fingers acquired via five channels made of the MF-TENG.

and PDA-CNTs are found to be 98.4% and 75.3%, respectively. As the weight loss for the CNTs is 1.6%, the weight loss for PDA is found to be 23.1%. Up to now, the exact mechanism of the PDA action is still unclear. One possibility may be that the protons of the dihydroxy group in DA generate 5,6-dihydroxyindole (DHI), which then further oxidizes and polymerizes to form PDA. The self-healing process of the PDA-CNTs/PVA hydrogel can be described in terms of both physical and chemical mechanisms. From the perspective of the physical mechanism, after the PDA-CNTs/PVA hydrogel was divided into two parts, the photothermal activity of PDA and the CNTs in the PDA-CNTs/PVA hydrogel caused by the stimulation of the NIR laser radiation raised the temperature of the PDA-CNTs/PVA hydrogel within a short time. Then, the crystallites in PVA begin to melt, and the molecules of the PVA chains reorganize, resulting in the PDA-CNTs/PVA hydrogel gradually healing itself in the damaged area. From the perspective of the chemical mechanism, the borate ions are complexed with the hydroxyl groups of the PVA crystal, permitting the chemical self-healing process to occur, as shown in Figure 1c. In addition, the catechol and amino groups in PDA could form reversible hydrogen bonds with the hydroxyl groups in PVA. These factors simultaneously endow the PDA-CNTs/

PVA hydrogel with excellent self-healing ability. Owing to the strong interface interaction between the PDA-CNTs and the hydrogel, the PDA-CNTs are uniformly dispersed in the matrix, forming the conductive network, and enhance the conductivity of the PDA-CNTs/PVA hydrogel, as shown in the scanning electron microscopy (SEM) image (Figure 1d). On the other hand, we deposited Ag nanoparticles (NPs) on the surface of the PDA-CNTs and observed the dispersion of the Ag element in the hydrogel through electronic data switching (EDS) to demonstrate the dispersion of the PDA-CNTs in the PVA matrix (SI Figure S2). The Ag-PDA-CNTs/PVA hydrogel was prepared as follows. First, a certain amount of the PDA-CNTs and AgNO₃ solution were mixed in an alkaline solution under stirring for 12 h. Due to the weak reducibility of dopamine, silver NPs were deposited on the surface of the PDA-CNTs via a reductive reaction to form a hybrid filler (denoted as Ag-PDA-CNTs). Then, the Ag-PDA-CNTs were dispersed into the PVA hydrogel to form the Ag-PDA-CNTs/PVA composite. From SI Figure S2, it can be observed that the Ag element is aligned and uniformly dispersed, which demonstrates that the PDA-CNTs are well dispersed in the PVA matrix. It should be noted that, in the absence of external stimuli, the PDA-CNTs/PVA hydrogel could not only rebuild its structure but also resume its

conductive behavior within a short time, which can be demonstrated by connecting the PDA-CNTs/PVA hydrogel and a light-emitting diode (LED) within the same circuit (SI Figure S3a and SI Video S1). When the PDA-CNTs/PVA hydrogel was cut, the LED could not be lit. However, when the cross sections were again put in complete contact, the hydroxyl groups and borate ions between the cross sections quickly recombined to form hydroxyl bonds and borate ester bonds, thus resulting in a fully recovered PDA-CNTs/PVA hydrogel. Although the PDA-CNTs do not intrinsically possess a self-healing ability, they could be put back in contact through the self-healing process of the PDA-CNTs/PVA hydrogel, which restored the conductivity. As a result, the self-healed PVA hydrogel could light the LED again. In addition, the electrical resistance of the PDA-CNTs/PVA hydrogel before and after self-healing was tested, and the results showed that the original electrical resistance was 7.65 MΩ, while the self-healed PDA-CNTs/PVA hydrogel had a resistance of 7.80 MΩ. This indicates that the conductivity of the PDA-CNTs/PVA hydrogel remains almost the same after self-healing. This result demonstrates the excellent self-healing ability and electrical conductivity of the PDA-CNTs/PVA hydrogel. In addition, the PDA-CNTs/PVA hydrogel displayed a relatively good self-healing ability in a water environment. As shown in SI Figure S3b, when water was dropped onto the cut PDA-CNTs/PVA hydrogel, the cross sections of the PDA-CNTs/PVA hydrogel could still be joined together. However, some defects occurred at the joint, which can be ascribed to the PDA-CNTs/PVA hydrogel absorbing some water and swelling, hindering the full formation of the dynamic borate ester bonds. Figure 1e shows the stress−strain curves of pure PVA as well as of the original and self-healed PDA-CNTs/PVA hydrogel. The tensile strain and strength of the original PDA-CNTs/PVA hydrogel reached 450% and 0.44 KPa, respectively, owing to the reinforcing effect of the PDA-CNTs. As shown in SI Video S2, a highly stretchable PDA-CNTs/PVA hydrogel (stretch ratio λ = 3) was obtained. Without external stimuli and within 10 min of self-healing, the tensile strain of the self-healed PDA-CNTs/PVA hydrogel reached 388%, illustrating that the self-healing rate of the PDA-CNTs/PVA hydrogel is 86% (Figure 1e). Figure 1f shows the preparation process of the MF-TENG, which consists in sandwiching the PDA-CNTs/PVA hydrogel between two self-healing silicone elastomer films.

The basic working mechanism and electrical output performance of the MF-TENG are shown in Figure 2. The as-prepared MF-TENG works in a single-electrode mode under the coupling between triboelectrification and electrostatic induction (Figure 2a). When the MF-TENG contacts the skin, electrification occurs at the contact interface, and a large number of charges with opposite polarity are generated (Figure 2a (i)). Due to the higher surface electron affinity of the silicone elastomer, the human skin surface is positively charged. The surface charge density of the triboelectric layer plays a critical role in achieving a high output performance of TENG. Improving the relative permittivity of triboelectric layer is beneficial for improving the output performance of TENG. However, when the conductivity of triboelectric layer increases and there is percolation in the triboelectric layer, the output performance of TENG decreases.[45] When the skin is separated from the MF-TENG, positive charges are generated in the PDA-CNTs/PVA hydrogel, which are inside the MF-TENG (Figure 2a (ii)). At this time, electrons from the hydrogel flow to the ground through an external circuit and generate an electrical signal.

When the skin and MF-TENG are completely separated, the positive charges in the hydrogel and negative charges in the silicone elastomer layer are balanced; thus, there is no electron flow in the external circuit (Figure 2a (iii)). When the skin moves back again, the electrons flow from the ground to the electrode through an external circuit, generating an electrical signal in the opposite direction (Figure 2a (iv)). Therefore, the role of the conductive triboelectric layer in terms of the electrical output performance is that of inducing an electric charge and acting as a wire. The triboelectric performance of the self-healing silicone elastomer was tested using a linear motor, and the corresponding results are shown in SI Figure S4. During testing, the self-healing silicone elastomer acts as a triboelectric layer, while a copper foil (30 × 30 mm^2) was used as another triboelectric layer. From SI Figure S4, it can be found that the open-circuit voltage (V_{oc}), the peak value of the short-circuit current (I_{sc}), and the transfer charge (Q_{sc}) of the self-healing silicone elastomer are 50.1 V, 6.9 μA, and 63.3 nC, respectively. As shown in Figures 2b (i) and (ii), the corresponding V_{oc} values of the original and self-healed MF-TENGs are 38.57 and 37.17 V, respectively. In addition, the peak values of I_{sc} of the original and self-healed MF-TENGs are 7.98 and 6.28 μA, respectively, as shown in SI Figure S5a. The Q_{sc} values of the original and self-healed MF-TENGs are 78.34 and 62.53 nC, respectively. The comparison of the electrical output performance between the original and self-healed MF-TENGs is shown in SI Table S1. From Figure 2b and SI Table S1, it is found that the self-healed V_{oc} is slightly less than the original V_{oc}, which is ascribed to the fact that the surface characteristics and inner structure of the MF-TENG do not recover their original state completely. However, the self-healed and original V_{oc} values are of the same order of magnitude, indicating the highly efficient self-healing ability of the prepared nanogenerator. In addition, the durability of the MF-TENG was measured, and the V_{oc}, I_{sc}, and Q_{sc} values remain almost the same over 500 cycles, demonstrating the highly stable electrical output performance of the MF-TENG (SI Figure S6). Moreover, the MF-TENG was used to charge a 2.2 μF capacitor by using a linear motor, and the result is shown in SI Figure S7. It can be seen that the MF-TENG increased the voltage from 0 to 2 V and continuously charged the capacitor for around 300 s. Figure 2c shows an application of the MF-TENG in the wearable technology field. A smart electronic data glove that could detect human gestures was prepared. The electronic data glove combined five MF-TENGs, which were connected to different human fingers. Due to the low cross-linking density of self-healing silicone elastomer, MF-TENG can be adhered to human skin within a short time. However, the repeated bending of human joints, sweat, and air humidity will decrease the adhesion ability of MF-TENG. As a result, we used tape to fix the MF-TENG on fingers during the repeated testing. A customized data acquisition system with five channels and a real-time analysis software capturing and displaying the electrical signals on the computer was developed in conjunction with the smart electronic data glove. The electrical signals generated by human gestures were tested through each channel. When one finger was bent, the voltage of the corresponding channel in the MF-TENG increased significantly, while the voltage of the other channels remained in the original state. In the future, this smart electronic data glove could be used in conjunction with artificial intelligence. Furthermore, the recognition of more complex gestures could be achieved through machine learning and self-training. This smart electronic data glove could help blind people to type on a keyboard or convert language into a
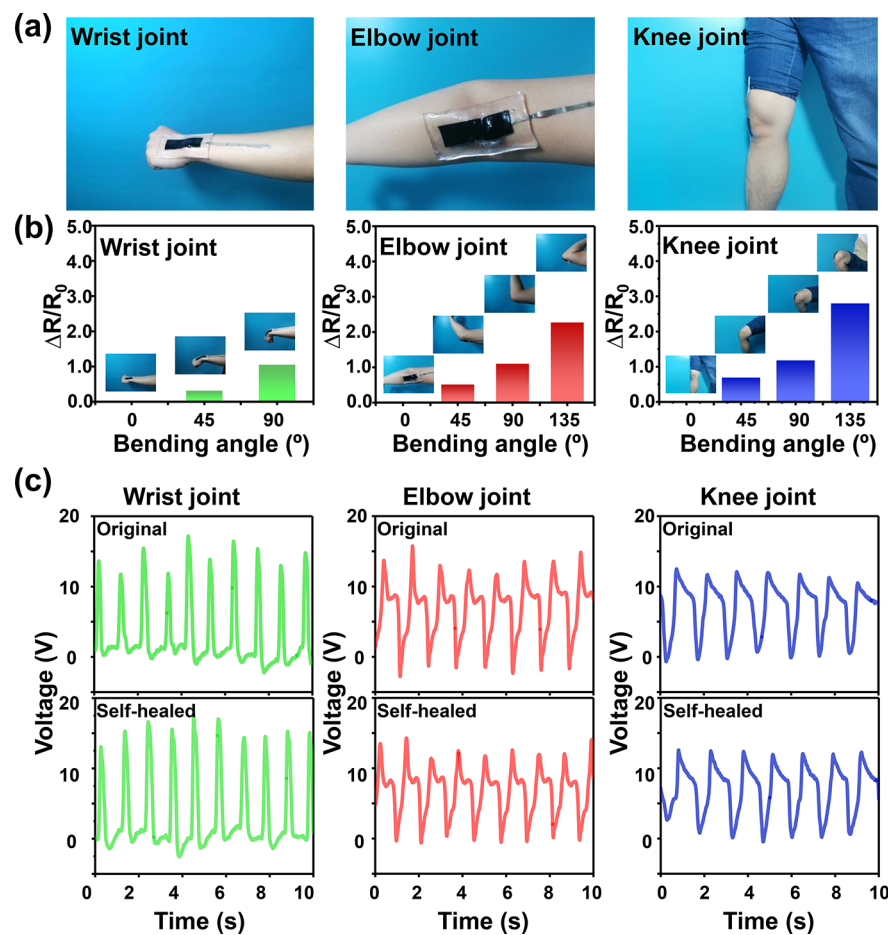
Figure 3. Application of the MF-TENG to different joints of a human body for large-scale human motion. (a) Photos of the MF-TENG attached to different joints of the human body; (b) Relative resistance variations of the MF-TENG attached to the wrist, elbow, and knee joints motion at different bending angles; (c) Open-circuit voltage of the original and self-healed MF-TENG for the wrist, elbow, and knee joints motion at the ultimate bending angle, respectively.

machine-recognizable language and output the corresponding sound. Besides the excellent self-healing ability, the prepared MF-TENG exhibited a good shape tunability, which could further expand its application. As shown in SI Figure S8a, the original device was cut into many squares with the same size, which could be assembled into different MF-TENG shapes (shapes 1−4) via the self-healing process. SI Figure S8b shows the V_{oc} and I_{sc} of the original MF-TENG and the MF-TENG with different shapes, respectively. All the different MF-TENG shapes exhibited an output electrical performance similar to that of the original device. The V_{oc} and I_{sc} values of the MF-TENG with different shapes were restored to about 39 V and 5.3 μA (SI Figure S8b), respectively, demonstrating the excellent shape tunability of the MF-TENG.

In order to further explore the application of the MF-TENG in real life, the as-prepared device was mounted on a human elbow, knee, and wrist joints (Figure 3a). It can be seen that the MF-TENG can be adhered to these joints and changed its deformation to adapt to the joint motion. As the bending angle increased, the distance between the conductive PDA-CNTs in the matrix increased, resulting in a greater change in the relative resistance of the MF-TENG. Therefore, the relative resistance change in the MF-TENG (i.e., $\Delta R/R_0 = (R_m - R_0)/R_0$, where R_m and R_0 correspond to the real-time resistance and initial resistance during the measurement process, respectively) was measured under different bending angles for three human joints

(namely, the wrist, elbow, and knee joints (Figure 3b)) to evaluate their health. When the wrist, elbow, and knee joints gradually bent to 45°, the relative resistance changes are 0.308, 0.509, and 0.685, respectively. With a bend angle of 90°, the relative resistance changes are 1.039, 1.102, and 1.167, respectively. When the elbow and knee joints bent to the bending angle of 135°, the relative resistance changes are 2.252 and 2.795, respectively. As the deformation increases, the resistance value of the device increases. Although the device is bent up to 90° at different joints, the deformation of the device is different. The deformation of the MF-TENG at the wrist joint is the smallest, while that at the knee joint is the largest. The effect of the relative change in resistance of the PDA-CNTs/PVA hydrogel on the electrical output performance of the TENG is shown in SI Figure S9. Compared with the initial state ($\lambda = 1$), there is a slight decline (∼30%) in electrical output performance after the MF-TENG is stretched to $\lambda = 1.5$, which is attributed to the resistance increment of the PVA hydrogel electrode. However, when the MF-TENG recovers to the stretched state, the electrical output performance is comparable with the initial value, indicating no degradation of the MF-TENG. Therefore, based on the change in the relative resistance, the MF-TENG could be applied to detect the recovery state of the injured joint. If the damaged human joint was fully recovered, the $\Delta R/R_0$ ratio would recover the value of a healthy human joint. In addition, the MF-TENG could be used to convert the mechanical energy
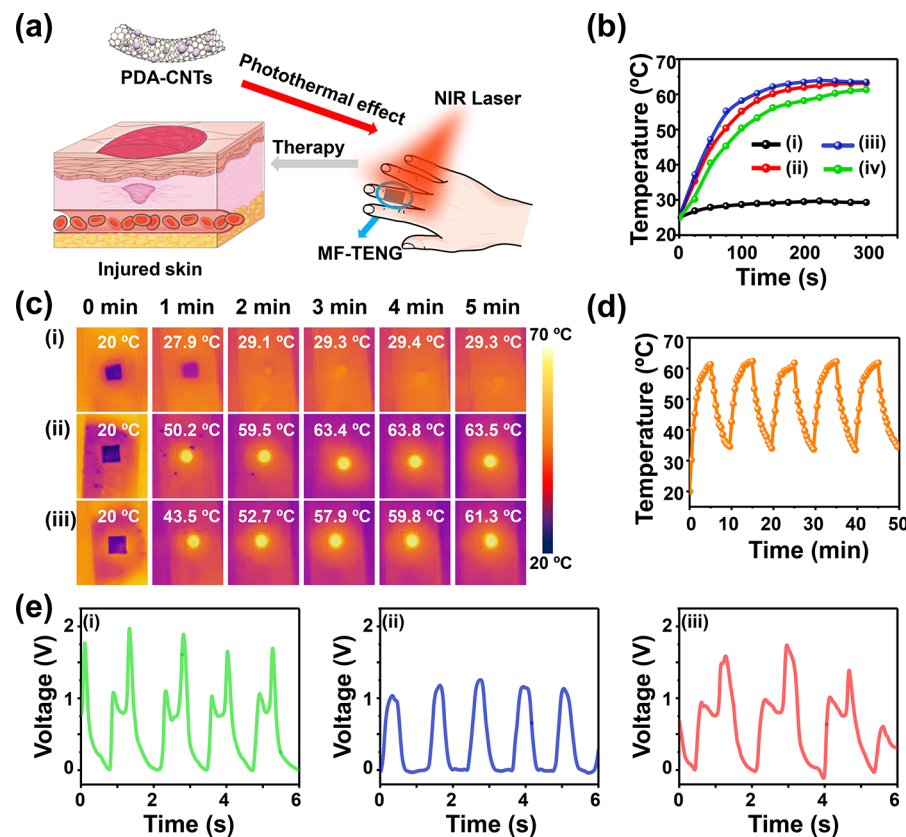
Figure 4. (a) Simulation diagram of the photothermal treatment; (b) Photothermal curves of (i) pure PVA, (ii) the CNTs/PVA hydrogel, (iii) the PDA-CNTs/PVA hydrogel, and (iv) the MF-TENG under exposure to NIR laser light with a power density of 1 W/cm^2; (c) Photothermal images of (i) pure PVA, (ii) the PDA-CNTs/PVA hydrogel, and (iii) the MF-TENG; (d) Photothermic stability of the MF-TENG under laser irradiation with a power density of 1 W/cm^2 for five on/off cycles; (e) Bending detection of the finger in (i) the healthy state, (ii) the injured state, and (iii) at completion of the photothermal treatment.

collected from the motion of the human joints into electrical energy and output the corresponding electrical signals. Figure 3c shows the V_{oc} values of the original and self-healed MF-TENG for the wrist, elbow, and knee joints motion at the ultimate bending angle, respectively, displaying a relatively high stability. In addition, it can be seen from SI Figure S10a,b that the I_{sc} and the average Q_{sc} values of original and self-healed MF-TENG for the wrist, elbow, and knee joints motion at the ultimate bending angle are also relatively stable within a certain range. It is worth noting that, after the MF-TENG was cut using a commercial blade, the output electrical performance of the self-healed MF-TENG on the human joints recovered its initial state, which is ascribed to the excellent self-healing ability of the MF-TENG (Figures 3c, SI Figure S10a,b).

It was interesting to find that the PDA-CNTs in the matrix could not only enhance the mechanical strength of the PDA-CNTs/PVA hydrogel, but it also acted as a photothermal conversion agent for increasing the temperature of the MF-TENG. The increased temperature is a benefit to accelerate the microcirculatory blood flow and relieve pain in the injured area when exposed to NIR laser light[46−48] (Figure 4a). From Figure 4b, it can be observed that the temperature of the PDA-CNTs/PVA hydrogel increased from 25 to 62 °C within 5 min under 808 nm laser irradiation (1 W/cm^2). However, the heating rate of the MF-TENG was less than that of the PDA-CNTs/PVA hydrogel in the same conditions, which is attributed to the poor thermal conductivity of the self-healing silicone elastomer on the outer of the PDA-CNTs/PVA hydrogel. By contrast, the low

heating rate is beneficial for avoiding burning of the skin around the wound within a short time (Figure 4c). As shown in Figure 4d, the MF-TENG exhibits a stable photothermal performance over five laser on/off heating cycles. In order to further verify the effect of photothermal treatment, we adhered the MF-TENG on the finger and tested the blood flow velocity in fingertip before and after laser irradiation. The result showed that the blood flow velocity of fingertip is 482 μm/s on 37 °C. However, the blood flow velocity increased to 557 μm/s when the temperature of fingertip increased to 60 °C after photothermal treatment. In addition, the MF-TENG was placed on an injured finger for detection and treatment. Figures 4e (i), (ii), and (iii) show the output voltage and waveform when the finger is in a healthy state, injured state, and at completion of the photothermal treatment, respectively. Compared with the single-peak waveform of the injured state, the double-peak waveform of the healthy state and of the state at completion of the photothermal treatment indicates that complete motion of the finger joints is possible. At the same time, the voltage after treatment is 1.78 V, which is close to the value of the healthy finger joint (1.97 V), proving that the MF-TENG has a photothermal treatment ability and can assist the recovery of finger joint motion. We also tested in real time the V_{oc} of the finger joints in fully bent and semibent states (SI Video S3). From SI Video S3, a bimodal voltage waveform can be seen when the finger is fully bent, while a single-peak voltage waveform is found when the finger is semibent. However, when the finger is extended with rest without motion, the detection machine displays a horizontal

signal. In addition, the cell viability of PVA and the PDA-CNTs/PVA hydrogel as a function of the incubation time is displayed in SI Figure S11, indicating their good biocompatibility. Due to the fact that the PVA hydrogel and self-healing silicone elastomer are not biodegradable, the MF-TENG does not possess biodegradability. In recent several years, biodegradable materials have been widely applied in flexible wearable electronic devices due to their biodegradability, biocompatibility, and recyclability. In our future researches, we will try to develop biodegradable materials and apply them on the flexible wearable electronic devices.

CONCLUSIONS

A self-healing and elastic MF-TENG, consisting of a thin conductive self-healing PDA-CNTs/PVA hydrogel sandwiched between two healable silicone elastomer films was successfully prepared. In the self-healing PDA-CNTs/PVA hydrogel, the sodium borate provided reversible healing sites, while the PDA-CNTs endowed it with high electrical conductivity and photothermal properties. In addition, the PDA-CNTs/PVA hydrogel exhibited excellent mechanical properties with a large tensile strain of 450%. This MF-TENG could be easily tailored and implemented into devices wearable on different joints of the human body to collect health information, which can be used to determine the recovery state of the joints by comparing electrical output performance. It is worth mentioning that, with NIR laser irradiation, the temperature of the MF-TENG could increase gradually from 25 to 60 °C in 5 min, which could provide a photothermal therapy. Owing to its excellent self-healing properties, capability to monitor human joint health, and excellent photothermal properties, this MF-TENG could be widely used in health and exercise monitors, soft robots, and wearable electronics.

EXPERIMENTAL METHODS

Materials. DA ($C_{18}H_{11}NO_2 \cdot HCl$, 98%) and Tris ($C_4H_{11}NO_3$, 99%) were obtained from the Sigma-Aldrich Corp. CNTs were purchased from Chengdu Institute of Physics and Chemistry. Poly(vinyl alcohol) (PVA-1799) was purchased from Macleans Chemical Reagent Co., Ltd. The self-healing silicone elastomer (AD-549) was obtained from Guangzhou Xinguan Chemical Co., Ltd. Sodium tetraborate decahydrate ($Na_2B_4O_7 \cdot 10H_2O$) and 1,4-Phthalaldehyde (623−27−8) were commercial products.

In Situ **Polymerization of DA Deposited onto the CNTs.** The pristine CNTs (0.2 g) were first immersed in 100 mL of DA solution (2.0 mg/mL, 0.125 g Tris, pH 8.5) and left under vigorous magnetic stirring for 24 h. Next, the as-formed PDA-CNTs were filtered off through a cellulose filter paper and dried in a vacuum oven at 60 °C.

Fabrication of the Self-Healing PDA-CNTs/PVA Hydrogel. PVA-1799 (6 g) and PDA-CNTs (0.2 g) were mixed with 55 mL of deionized water. Then, the temperature was increased to 110 °C, and the mixture was stirred for 5 h until a gel-like mixture was obtained. Next, the $Na_2B_4O_7 \cdot 10H_2O$ solution was directly added to the gel-like mixture, and stirred at 95 °C for another 5 min. Then, the PDA-CNTs/PVA hydrogel was poured into a hollow steel plate mold with a height of 1.0 mm, and a 20 kg load was pressed on the hollow steel plate mold for 2 min. Then, the self-healing PDA-CNTs/PVA hydrogel was placed into the mold for a freezing/thawing treatment (freezing at −20 °C for 1 h followed by defrosting at room temperature for 6 h). Finally, the freezing/thawing procedure was performed one to three times to obtain the final product.

Fabrication of the MF-TENG. In a previous study, we developed a self-healing silicone elastomer based on dynamic imine bonds, which could self-heal within 0.5 h under no external stimulus.[49] This self-healing silicone elastomer with an electrical resistance of 2.24×10^{11} Ω was used as the synthetic platforms for the present study. First, the poly(amine-dimethylsiloxane) (PDMS-NH$_2$) and curing agent (terephthalaldehyde) were mixed in a ratio of 200:1 (m/m); then, the mixture was coated onto a mold with a thickness of around 1.0 mm. The dynamic imine bonds in self-healing silicone elastomer act as both the polymer cross-linking and self-healing points of the PDMS-NH$_2$ networks. Next, a piece of the self-healing PDA-CNTs/PVA hydrogel with a certain size was placed on top of the previous self-healing silicone elastomer. Then, another layer of the self-healing silicone elastomer with a thickness of about 1.0 mm was coated onto the surface of the PDA-CNTs/PVA hydrogel to form the MF-TENG with a sandwich structure. The dimension of the MF-TENG is $40.0 \times 40.0 \times 3.0$ mm^3, while the dimension of the within PDA-CNTs/PVA hydrogel is $30.0 \times 30.0 \times 1.0$ mm^3. The dimension of the MF-TENG attached at different human joints (wrist, elbow, and knee joints) is $90.0 \times 45.0 \times 3.0$ mm^3, while the dimension of the within PDA-CNTs/PVA hydrogel is $70.0 \times 20.0 \times 1.0$ mm^3. The dimension of the MF-TENG attached at finger joints is $40.0 \times 20.0 \times 3.0$ mm^3, while the dimension of the within PDA-CNTs/PVA hydrogel is $25.0 \times 10.0 \times 1.0$ mm^3.

Measurements and Characterization. The typical electrical output performance of the MF-TENG and self-healing silicone elastomer was measured by using a linear motor at 1.5 Hz and 2 cm and a Keithley electrometer 6514. The electrical output performance of the MF-TENG on human joints were recorded using a Keithley electrometer 6514. The SEM and EDS images were acquired using a Zeiss Gemin300. The stress−strain curves of dumbbell samples were measured using an Instron 3366 testing machine. The maximum test stress is 10 kN, and the tensile speed is 50 mm/min. The samples have a width of 6 mm, a thickness of 1 mm, and a standard distance of 60 mm. The self-healing PDA-CNTs/PVA hydrogel was exposed to the 808 nm laser with a power density of 1 W/cm^2. The temperature changes of the self-healing PDA-CNTs/PVA hydrogel were recorded using a thermal infrared imaging camera (Flirone pro). Cell viability was measured using MTT assays.

ASSOCIATED CONTENT

SI **Supporting Information**

The Supporting Information is available free of charge at https://pubs.acs.org/doi/10.1021/acsnano.1c04384.

> Figures S1−S11 show the TGA curves, SEM and EDS images, electrical output performance, optical and digital images, and cell viability of the MF-TENG. Table S1 compares the electrical output performance between the original and self-healed MF-TENGs (PDF)

> Video S1 shows the conductive behavior of self-healing of the PDA-CNTs/PVA hydrogel (AVI)

> Video S2 shows the tensile property of self-healing of the PDA-CNTs/PVA hydrogel (AVI)

> Video S3 shows real-time monitoring of finger motion using the MF-TENG (AVI)

AUTHOR INFORMATION

Corresponding Author

Zhong Lin Wang — *School of Material Science and Engineering, Georgia Institute of Technology, Atlanta, Georgia 30332-0245, United States; Beijing Key Laboratory of Micro-nano Energy and Sensor, Beijing Institute of Nanoenergy and Nanosystems, Chinese Academy of Sciences, Beijing 100083, P. R. China;* ⓘ orcid.org/0000-0002-5530-0380; Email: zhong.wang@mse.gatech.edu

Authors

Dan Yang — *Beijing Key Lab of Special Elastomeric Composite Materials, Department of Material Science and Engineering, Beijing Institute of Petrochemical Technology, Beijing 102617, P. R. China; Department of Materials Science and Engineering, Beijing University of Chemical Technology, Beijing 100029, P.*

R. China; School of Material Science and Engineering, Georgia Institute of Technology, Atlanta, Georgia 30332-0245, United States; ⓞ orcid.org/0000-0002-5409-2559

Yufeng Ni − Beijing Key Lab of Special Elastomeric Composite Materials, Department of Material Science and Engineering, Beijing Institute of Petrochemical Technology, Beijing 102617, P. R. China

Xinxin Kong − Beijing Key Lab of Special Elastomeric Composite Materials, Department of Material Science and Engineering, Beijing Institute of Petrochemical Technology, Beijing 102617, P. R. China

Shuyao Li − Beijing Key Laboratory of Micro-nano Energy and Sensor, Beijing Institute of Nanoenergy and Nanosystems, Chinese Academy of Sciences, Beijing 100083, P. R. China

Xiangyu Chen − Beijing Key Laboratory of Micro-nano Energy and Sensor, Beijing Institute of Nanoenergy and Nanosystems, Chinese Academy of Sciences, Beijing 100083, P. R. China; ⓞ orcid.org/0000-0002-0711-0275

Liqun Zhang − Department of Materials Science and Engineering, Beijing University of Chemical Technology, Beijing 100029, P. R. China; ⓞ orcid.org/0000-0002-2103-6294

Complete contact information is available at:
https://pubs.acs.org/10.1021/acsnano.1c04384

Notes
The authors declare no competing financial interest.

REFERENCES

(1) Zhang, J. H.; Li, Y.; Du, J.; Hao, X.; Wang, Q. Bio-Inspired Hydrophobic/Cancellous/Cydrophilic Trimurti PVDF Mat-Based Wearable Triboelectric Nanogenerator Designed by Self-Assembly of Electropore-Pore-Creating. Nano Energy **2019**, 61, 486−495.

(2) Wang, Z. L. Self-Powered Nanosensors and Nanosystems. Adv. Mater. **2012**, 24, 280−285.

(3) Wang, Z. L. Triboelectric Nanogenerators as New Energy Technology for Self-Powered Systems and as Active Mechanical and Chemical Sensors. ACS Nano **2013**, 7, 9533−9557.

(4) Guo, H.; Pu, X.; Chen, J.; Meng, Y.; Yeh, M. H.; Liu, G.; Tang, Q.; Chen, B.; Liu, D.; Qi, S.; Wu, C.; Hu, C.; Wang, J.; Wang, Z. L. A Highly Sensitive, Self-Powered Triboelectric Auditory Sensor for Social Robotics and Hearing Aids. Sci. Robot. **2018**, 3, No. eaat2516.

(5) Chen, J.; Guo, H.; He, X.; Liu, G.; Xi, Y.; Shi, H.; Hu, C. Enhancing Performance of Triboelectric Nanogenerator by Filling High Dielectric Nanoparticles into Sponge PDMS Film. ACS Appl. Mater. Interfaces **2016**, 8, 736−744.

(6) Nie, J.; Ren, Z.; Xu, L.; Lin, S.; Zhan, F.; Chen, X.; Wang, Z. L. Probing Contact-Electrification-Induced Electron and Ion Transfers at a Liquid-Solid Interface. Adv. Mater. **2020**, 32, 1905696.

(7) Shi, Y.; Wang, F.; Tian, J.; Li, S.; Fu, E.; Nie, J.; Lei, R.; Ding, Y.; Chen, X.; Wang, Z. L. Self-Powered Electro-Tactile System for Virtual Tactile Experiences. Sci. Adv. **2021**, 7, No. eabe2943.

(8) Guan, Q. B.; Dai, Y. H.; Yang, Y. Q.; Bi, X. Y.; Wen, Z.; Pan, Y. Near-Infrared Irradiation Induced Remote and Efficient Self-Healable Triboelectric Nanogenerator for Potential Implantable Electronics. Nano Energy **2018**, 51, 333−339.

(9) Kong, X.; Yang, D.; Ni, Y.; Hao, J.; Guo, W.; Zhang, L. Enhanced Actuation Strains of Rubber Composites by Combined Covalent and Noncovalent Modification of TiO_2 Nanoparticles. Ind. Eng. Chem. Res. **2019**, 58, 19890−19898.

(10) Lei, R.; Shi, Y.; Ding, Y.; Nie, J.; Li, S.; Wang, F.; Zhai, H.; Chen, X.; Wang, Z. L. Sustainable High-Voltage Source Based on Triboelectric Nanogenerator with a Charge Accumulation Strategy. Energy Environ. Sci. **2020**, 13, 2178−2190.

(11) Bai, Z.; Zhang, Z.; Li, J.; Guo, J. Textile-Based Triboelectric Nanogenerators with High-Performance via Optimized Functional Elastomer Composited Tribomaterials as Wearable Power Source. Nano Energy **2019**, 65, 104012.

(12) Chen, S.; Huang, T.; Zuo, H.; Qian, S.; Guo, Y.; Sun, L.; Lei, D.; Wu, Q.; Zhu, B.; He, C.; Mo, X.; Jeffries, E.; Yu, H.; You, Z. A Single Integrated 3D-Printing Process Customizes Elastic and Sustainable Triboelectric Nanogenerators for Wearable Electronics. Adv. Funct. Mater. **2018**, 28, 1805108.

(13) Mariello, M.; Fachechi, L.; Guido, F.; De Vittorio, M. Conformal, Ultra-Thin Skin-Contact-Actuated Hybrid Piezo/Triboelectric Wearable Sensor Based on AlN and Parylene-Encapsulated Elastomeric Blend. Adv. Funct. Mater. **2021**, 31, 2101047.

(14) Peng, X.; Dong, K.; Ning, C.; Cheng, R.; Yi, J.; Zhang, Y.; Sheng, F.; Wu, Z.; Wang, Z. L. All-Nanofiber Self-Powered Skin-Interfaced Real-Time Respiratory Monitoring System for Obstructive Sleep Apnea-Hypopnea Syndrome Diagnosing. Adv. Funct. Mater. **2021**, 31, 2103559.

(15) Lee, S.; Ko, W.; Oh, Y.; Lee, J.; Baek, G.; Lee, Y.; Sohn, J.; Cha, S.; Kim, J.; Park, J.; Hong, J. Triboelectric Energy Harvester Based on Wearable Textile Platforms Employing Various Surface Morphologies. Nano Energy **2015**, 12, 410−418.

(16) Pu, X.; Li, L.; Song, H.; Du, C.; Zhao, Z.; Jiang, C.; Cao, G.; Hu, W.; Wang, Z. L. A Self-Charging Power Unit by Integration of a Textile Triboelectric Nanogenerator and a Flexible Lithium-Ion Battery for Wearable Electronics. Adv. Mater. **2015**, 27, 2472−2478.

(17) Zhong, Q.; Zhong, J.; Hu, B.; Hu, Q.; Zhou, J.; Wang, Z. L. A Paper-Based Nanogenerator as a Power Source and Active Sensor. Energy Environ. Sci. **2013**, 6, 1779−1784.

(18) Dai, X.; Huang, L. B.; Du, Y.; Han, J.; Zheng, Q.; Kong, J.; Hao, J. Self-Healing, Flexible, and Tailorable Triboelectric Nanogenerators for Self-Powered Sensors Based on Thermal Effect of Infrared Radiation. Adv. Funct. Mater. **2020**, 30, 1910723.

(19) Guan, Q.; Lin, G.; Gong, Y.; Wang, J.; Tan, W.; Bao, D.; Liu, Y.; You, Z.; Sun, X.; Wen, Z.; Pan, Y. Highly Efficient Self-Healable and Dual Responsive Hydrogel-Based Deformable Triboelectric Nanogenerators for Wearable Electronics. J. Mater. Chem. A **2019**, 7, 13948−13955.

(20) Chen, Y.; Zhang, Y.; Zhan, T.; Lin, Z.; Zhang, S. L.; Zou, H.; Zhang, G.; Zou, C.; Wang, Z. L. An Elastic Triboelectric Nanogenerator for Harvesting Random Mechanical Energy with Multiple Working Modes. Adv. Mater. Technol. **2019**, 4, 1900075.

(21) Jin, L.; Chen, J.; Zhang, B.; Deng, W.; Zhang, L.; Zhang, H.; Huang, X.; Zhu, M.; Yang, W.; Wang, Z. L. Self-Powered Safety Helmet Based on Hybridized Nanogenerator for Emergency. ACS Nano **2016**, 10, 7874−7881.

(22) Bhatta, T.; Maharjan, P.; Salauddin, M.; Rahman, M. T.; Rana, S. S.; Park, J. Y. A Battery-Less Arbitrary Motion Sensing System Using Magnetic Repulsion-Based Self-Powered Motion Sensors and Hybrid Nanogenerator. Adv. Funct. Mater. **2020**, 30, 2003276.

(23) Li, G. Z.; Wang, G. G.; Ye, D. M.; Zhang, X. W.; Lin, Z. Q.; Zhou, H. L.; Li, F.; Wang, B. L.; Han, J. C. High-Performance Transparent and Flexible Triboelectric Nanogenerators Based on PDMS-PTFE Composite Films. Adv. Electron. Mater. **2019**, 5, 1800846.

(24) Mi, H. Y.; Jing, X.; Zheng, Q.; Fang, L.; Huang, H. X.; Turng, L. S.; Gong, S. High-Performance Flexible Triboelectric Nanogenerator Based on Porous Aerogels and Electrospun Nanofibers for Energy

Harvesting and Sensitive Self-Powered Sensing. *Nano Energy* **2018**, *48*, 327−336.

(25) Yan, S.; Lu, J.; Song, W.; Xiao, R. Flexible Triboelectric Nanogenerator Based on Cost-Effective Thermoplastic Polymeric Nanofiber Membranes for Body-Motion Energy Harvesting with High Humidity-Resistance. *Nano Energy* **2018**, *48*, 248−255.

(26) Zhou, Q.; Park, J. G.; Kim, K. N.; Thokchom, A. K.; Bae, J.; Baik, J. M.; Kim, T. Transparent-Flexible-Multimodal Triboelectric Nanogenerators for Mechanical Energy Harvesting and Self-Powered Sensor Applications. *Nano Energy* **2018**, *48*, 471−480.

(27) Yang, J.; Chen, J.; Su, Y.; Jing, Q.; Li, Z.; Yi, F.; Wen, X.; Wang, Z.; Wang, Z. L. Eardrum-Inspired Active Sensors for Self-Powered Cardiovascular System Characterization and Throat-Attached Anti-Interference Voice Recognition. *Adv. Mater.* **2015**, *27*, 1316−1326.

(28) Luo, N.; Feng, Y.; Wang, D.; Zheng, Y.; Ye, Q.; Zhou, F.; Liu, M. New Self-Healing Triboelectric Nanogenerator Based on Simultaneous Repair Friction Layer and Conductive Layer. *ACS Appl. Mater. Interfaces* **2020**, *12*, 30390−30398.

(29) Cheng, B.; Wu, P. Scalable Fabrication of Kevlar/Ti$_3$C$_2$T$_x$ MXene Intelligent Wearable Fabrics with Multiple Sensory Capabilities. *ACS Nano* **2021**, *15*, 8676−8685.

(30) Xia, K.; Zhu, Z.; Zhang, H.; Du, C.; Xu, Z.; Wang, R. Painting a High-Output Triboelectric Nanogenerator on Paper for Harvesting Energy from Human Body Motion. *Nano Energy* **2018**, *50*, 571−580.

(31) Shi, X.; Wu, P. A Smart Patch with On-Demand Detachable Adhesion for Bioelectronics. *Small* **2021**, *17*, 2101220.

(32) Sun, H.; You, X.; Jiang, Y.; Guan, G.; Fang, X.; Deng, J.; Chen, P.; Luo, Y.; Peng, H. Self-Healable Electrically Conducting Wires for Wearable Microelectronics. *Angew. Chem., Int. Ed.* **2014**, *53*, 9526−9531.

(33) Cao, Y.; Morrissey, T. G.; Acome, E.; Allec, S. I.; Wong, B. M.; Keplinger, C.; Wang, C. A Transparent, Self-Healing, Highly Stretchable Ionic Conductor. *Adv. Mater.* **2017**, *29*, 1605099.

(34) Nie, J.; Wang, Z.; Ren, Z.; Li, S.; Chen, X.; Wang, Z. L. Power Generation from the Interaction of a Liquid Droplet and a Liquid Membrane. *Nat. Commun.* **2019**, *10*, 2264.

(35) Yang, D.; Guo, H.; Chen, X.; Wang, L.; Jiang, P.; Zhang, W.; Zhang, L.; Wang, Z. L. A Flexible and Wide Pressure Range Triboelectric Sensor Array for Real-Time Pressure Detection and Distribution Mapping. *J. Mater. Chem. A* **2020**, *8*, 23827−23833.

(36) He, F.; You, X.; Gong, H.; Yang, Y.; Bai, T.; Wang, W.; Guo, W.; Liu, X.; Ye, D. Stretchable, Biocompatible, and Multifunctional Silk Fibroin-Based Hydrogels Toward Wearable Strain/Pressure Sensors and Triboelectric Nanogenerators. *ACS Appl. Mater. Interfaces* **2020**, *12*, 6442−6450.

(37) Gogurla, N.; Roy, B.; Kim, S. Self-Powered Artificial Skin Made of Engineered Silk Protein Hydrogel. *Nano Energy* **2020**, *77*, 105242.

(38) Bhatta, T.; Pukar, M.; Cho, H.; Park, C.; Yoon, S. H.; Sharma, S.; Salauddin, M.; Rahman, M. T.; Rana, S. S.; Park, J. Y. High-Performance Triboelectric Nanogenerator Based on MXene Functionalized Polyvinylidene Fluoride Composite Nanofibers. *Nano Energy* **2021**, *81*, 105670.

(39) Peng, X.; Dong, K.; Ye, C.; Jiang, Y.; Zhai, S.; Cheng, R.; Liu, D.; Gao, X.; Wang, J.; Wang, Z. L. A Breathable, Biodegradable, Antibacterial, and Self-Powered Electronic Skin Based on All-Nanofiber Triboelectric Nanogenerators. *Sci. Adv.* **2020**, *6*, No. eaba9624.

(40) Deng, Z.; Hu, T.; Lei, Q.; He, J.; Ma, P. X.; Guo, B. Stimuli-Responsive Conductive Nanocomposite Hydrogels with High Stretchability, Self-Healing, Adhesiveness, and 3D Printability for Human Motion Sensing. *ACS Appl. Mater. Interfaces* **2019**, *11*, 6796−6808.

(41) Chen, Y.; Pu, X.; Liu, M.; Kuang, S.; Zhang, P.; Hua, Q.; Cong, Z.; Guo, W.; Hu, W.; Wang, Z. L. Shape-Adaptive, Self-Healable Triboelectric Nanogenerator with Enhanced Performances by Soft Solid-Solid Contact Electrification. *ACS Nano* **2019**, *13*, 8936−8945.

(42) Xu, W.; Huang, L. B.; Hao, J. Fully Self-Healing and Shape-Tailorable Triboelectric Nanogenerators Based on Healable Polymer and Magnetic-Assisted Electrode. *Nano Energy* **2014**, *40*, 399−407.

(43) Sun, J.; Pu, X.; Liu, M.; Yu, A.; Du, C.; Zhai, J.; Hu, W.; Wang, Z. L. Self-Healable, Stretchable, Transparent Triboelectric Nanogenerators as Soft Power Sources. *ACS Nano* **2018**, *12*, 6147−6155.

(44) Wang, H.; Cheng, H.; Huang, Y.; Yang, C.; Wang, D.; Li, C.; Qu, L. Transparent, Self-Healing, Arbitrary Tailorable Moist-Electric Film Generator. *Nano Energy* **2020**, *67*, 104238.

(45) Rana, S. M. S.; Zahed, M. A.; Rahman, M. T.; Salauddin, M.; Lee, S. H.; Park, C.; Maharjan, P.; Bhatta, T.; Shrestha, K.; Park, J. Y. Cobalt-Nanoporous Carbon Functionalized Nanocomposite-Based Triboelectric Nanogenerator for Contactless and Sustainable Self-Powered Sensor Systems. *Adv. Funct. Mater.* **2021**, 2105110.

(46) Ouyang, J.; Ji, X.; Zhang, X.; Feng, C.; Tang, Z.; Kong, N.; Xie, A.; Wang, J.; Sui, X.; Deng, L.; Liu, Y.; Kim, J. S.; Cao, Y.; Tao, W. *In Situ* Sprayed NIR-Responsive, Analgesic Black Phosphorus-Based Gel for Diabetic Ulcer Treatment. *Proc. Natl. Acad. Sci. U. S. A.* **2020**, *117*, 28667−28677.

(47) Sheng, L.; Zhang, Z.; Zhang, Y.; Wang, E.; Ma, B.; Xu, Q.; Ma, L.; Zhang, M.; Pei, G.; Chang, J. A Novel "Hot Spring"-Mimetic Hydrogel with Excellent Angiogenic Properties for Chronic Wound Healing. *Biomaterials* **2021**, *264*, 120414.

(48) Qiao, Y.; He, J.; Chen, W.; Yu, Y.; Li, W.; Du, Z.; Xie, T.; Ye, Y.; Hua, S. Y.; Zhong, D.; Yao, K.; Zhou, M. Light-Activatable Synergistic Therapy of Drug-Resistant Bacteria-Infected Cutaneous Chronic Wounds and Nonhealing Keratitis by Cupriferous Hollow Nanoshells. *ACS Nano* **2020**, *14*, 3299−3315.

(49) Yang, D.; Ni, Y. F.; Su, H.; Shi, Y.; Liu, Q.; Chen, X.; He, D. Hybrid Energy System Based on Solar Cell and Self-Healing/Self-Cleaning Triboelectric Nanogenerator. *Nano Energy* **2021**, *79*, 105394.